Upward transport of iron at the west shelf edge–slope of the Okinawa Trough in the East China Sea

Ryohei Sasayama, Nanako Hioki, Yuichiroh Morita, Yutaka Isoda, Keiri Imai, Atsushi Ooki, and Kenshi Kuma*

Faculty of Fisheries Sciences, Hokkaido University, 3–1–1 Minato, Hakodate, Hokkaido 041–8611, Japan

*Corresponding author: Kenshi Kuma,
Tel:+81–138–49–5081; Fax:+81–138–40–8870; E-mail: kuma@fish.hokudai.ac.jp

Abstract

We studied the behavior of chemical substances in the upper 300 m of the water column across the continental shelf–slope interface in the East China Sea off the Okinawa Trough. The behaviors of iron, inorganic nutrients, and humic-like fluorescent dissolved organic matter were strongly influenced by the extensive water exchange between the East China Sea and Kuroshio Current across the shelf break and slope via upwelling and frontal processes. We attributed the high humic-like fluorescent intensity at the subsurface of the shelf break and slope regions to the lateral supply of humic-like fluorescent dissolved organic matter from the shelf sediments to the outer shelf region due to the intrusion of shelf water into Kuroshio subsurface water. We found that the behavior of iron at the continental shelf–slope was remarkably different from the conservative mixing of inorganic nutrients and humic-like fluorescent dissolved organic matter. In deep and bottom waters at the shelf–slope, high total iron concentrations, which were closely related to water transmittance, possibly resulted from the swept transport of iron-rich resuspended sediments over the shelf floor from the slope by the invading Kuroshio Intermediate Water close to the bottom.

Keywords Iron supply; Chemical substances; Hydrographic data; Upwelling; Resuspension of sediments; Shelf break; Continental slope; Kuroshio; Okinawa Trough; East China Sea

1 Introduction

Ecosystems in marginal seas are strongly affected by the iron supply from the land and continental shelf region. Iron is generally supplied to surface water via riverine and atmospheric inputs, upwelling, and vertical mixing (e.g., de Baar et al. 2001). It has recently been reported that the lateral supply of iron from the continental margin is one of the most important sources of iron to the open ocean (e.g., Lam and Bishop 2008; Tanaka et al. 2012; Hioki et al. 2014). As a result of reductive dissolution of insoluble Fe(III) during microbial oxidation of organic matter in continental shelf sediments, there is a large dissolved Fe(II) flux out of such sediments which is a significant source of iron from the continental shelf. In addition, several studies from continental slope regions (e.g., McPhee-Shaw 2006; Nedelec et al. 2006; Fujita et al. 2010) suggest that much of the suspended sediment containing iron arrives after lateral transport within nepheloid layers from the continental slope into deep water, rather than by vertical settling from surface water. Their iron can subsequently be upwelled into surface waters (Elrod et al. 2004; Lohan and Bruland 2008; Chever et al. 2015). Coastal upwelling is an important source of bioavailable iron as well as macronutrients to surface waters and is the principal control of primary productivity in coastal upwelling ecosystems (Johnson et al. 2001; Bruland et al. 2001; Elrod et al. 2008; Biller et al. 2013).

The East China Sea can be divided into a large shallow continental shelf region characterized by high productivity and the Okinawa Trough, which is a back-arc rifting basin with a large section deeper than 1000 m and a maximum depth of approximately 2200 m. The Kuroshio Current intrudes into the surface layer of the Okinawa Trough eastward of Taiwan and then flows northeastward along the shelf break, where it mixes with shelf water, before flowing out through the Tokara Strait south of Kyushu. Extensive water exchange between the East China Sea and the Kuroshio Current occurs across the shelf break via upwelling and frontal processes (Su 1998). There is frequently

a well-developed pycnocline at the depths of 150–200 m near the shelf break and isohalines, isotherms, and isopycnals have been observed to rise towards the shelf, the suggestion being that there is upwelling of trough water along the shelf break (e.g., Chen et al. 1995; Han et al. 2001).

In the present study, we report the vertical distributions of iron, inorganic nutrients and humic-like fluorescent dissolved organic matter (humic-like FDOM) in the water column along two transects across the continental shelf–slope interface in the East China Sea off the Okinawa Trough. The waters of the continental slope and Okinawa Trough can be expected to have hydrographical characteristics intermediate between those of the western North Pacific and the continental shelf. We focused in particular on the behavior of iron, inorganic nutrients, and humic-like FDOM in the ocean boundary region of the East China Sea.

2 Materials and Methods

2.1 Sampling

Sampling was carried out aboard the *T/S Oshoro-Maru* of Hokkaido University between 1 and 4 July 2011 along two transects across the shelf-slope interface in the East China Sea off the Okinawa Trough. Hydrographic observations (salinity, temperature, and depth) were conducted in the upper 300 m of the water column at 7 stations (EA1–EA7) along the EA line and at 7 stations (EB1–EB7) along the EB line (Fig. 1 and Table 1) with a conductivity-temperature-depth (CTD) probe (SBE 19plus, Sea-Bird Electronics, Bellevue, USA). Seawater samples were collected from depths of 5–300 m at 4 stations (EA1, EA3, EA5, and EA7) along the EA line (27°09′–29°00′N, 126°00′–127°00′E) and at 4 stations (EB1, EB3, EB5, and EB7) along the EB line (29°43′N, 126°45′–128°15′E) (Fig. 1 and Table 1) using a CTD-rosette multiple sampler which housed twelve acid-cleaned, Teflon-coated 5-L Niskin X sampling bottles (General Oceanics, Miami,

USA). Seawater samples were gravity-filtered on deck for analyses of humic-like FDOM and dissolved iron (D-Fe) by connecting an acid-cleaned, 0.22-μm Durapore filter (Millipak 100; Millipore, Billerica, USA) to the Niskin X spigot. Unfiltered seawater samples were collected for determination of inorganic nutrients and total dissolvable iron (TD-Fe) concentrations. The samples (7–8 mL) for humic-like FDOM and nutrient analyses, which were collected in 10-mL acrylic tubes (Sanplatec, Osaka, Japan), were immediately frozen and kept below –20 °C in the dark (1–2 months) prior to analysis (e.g., Kitayama et al. 2009; Hioki et al. 2014, 2015). The filtered and unfiltered seawater samples (100 mL) used for D-Fe and TD-Fe analyses, respectively, were initially collected in acid-cleaned 125-mL low-density polyethylene (LDPE) bottles (Nalgene, New York, USA). The filtered and unfiltered iron samples were then acidified to pH 1.7–1.8 with addition of ultrapure grade HCl in a class 100 clean-air bench in a clean room on board. The acidified iron samples were allowed to stand at room temperature for at least 3 months prior to iron analysis (Bruland and Rue, 2001). Sample treatment in the present study was the same as in previous studies (e.g., Nishimura et al. 2012; Kuma et al. 2014; Hioki et al. 2014, 2015).

Beam transmittance (%) in the water column was measured with a single-channel transmissometer having a wavelength of 470 nm (bandwidth = ~20 nm) and a path length of 25 cm (WET Labs, Sun Valley, USA). Water transmittance (Tr) can be expressed as the formula $Tr = e^{-cx}$ where c is the beam attenuation coefficient and x is the path length. In this study, the vertical profiles of water transmittance in the water column were inversely related to those of water turbidity (Takata et al. 2008; Fujita et al. 2010; Kuma et al. 2014). In general, the water transmittance is related to the concentration of particulate material in the water although the exact relationship varies with the type of particles (suspended particles, phytoplankton, and bacteria) and dissolved organic matter present.

137 2.2 Nutrients and humic-like FDOM

138 Major nutrient (NO_3+NO_2, PO_4, and $Si(OH)_4$) concentrations were measured by a
139 Technicon AutoAnalyzer using CSK standard solutions for NO_3 and NO_2 (Wako Pure
140 Chemical Industries, Japan) and standard methods (Parsons et al. 1984). The analytical
141 precisions by repetitive measurement (n = 6) of nutrient standard were estimated to be
142 2.3% for NO_3+NO_2, 7.0% for PO_4, and 0.40% for $Si(OH)_4$. The lower limits for
143 determination were 0.1 μM for NO_3+NO_2, 0.05 μM for PO_4, and 1μM for $Si(OH)_4$.

144 Humic-like FDOM was quantified by measuring humic-like fluorescence intensity
145 (humic F-intensity) as reported in previous studies (e.g., Kitayama et al. 2009; Hioki et
146 al. 2014, 2015). After the frozen filtered samples in acrylic tubes were thawed and
147 warmed overnight to room temperature in the dark, the humic F-intensity was measured
148 in a 1-cm quartz cell by a fluorescence spectrophotometer (model F-2000, Hitachi,
149 Japan) with excitation/emission at 320 nm/420 nm, using 10-nm bandwidths (Hayase et
150 al. 1988; Hayase and Shinozuka 1995). Fluorescence intensity was expressed in terms
151 of quinine sulfate units (1 $QSU_{320/420}$ = 1 ppb quinine sulfate in 0.05 M H_2SO_4 with
152 excitation/emission at 320 nm/420 nm; Mopper and Schultz 1993).

153

154 2.3 Dissolved and total dissolvable iron

155 Acidified iron samples were adjusted to pH 3.2 with addition of 8.15 M quartz-distilled
156 formic acid–4.54 M ultrapure-grade ammonium buffer solution (0.8 mL per 100-mL
157 sample solution) in a class 100 clean-air bench. The iron concentrations (D-Fe and
158 TD-Fe) in buffered filtered and unfiltered samples were determined using an automated
159 iron analyzer (Kimoto Electric, Osaka, Japan) and a combination of 8-hydroxyquinoline
160 immobilized chelating resin concentration and luminol–hydrogen peroxide
161 chemiluminescence detection in a closed flow-through system (Obata et al. 1993) as
162 briefly described in previous studies (e.g., Kuma et al. 2014; Hioki et al. 2014, 2015).
163 The accuracy of this analysis was checked using Sampling and Analysis of Iron (SAFe)

reference standard seawater (pH 1.7–1.8). The D-Fe in the SAFe surface water (S) and deep intercalibration water (D1) were determined to be 0.10 ± 0.01 nM (n = 6) for S and 0.70 ± 0.03 nM (n = 5) for D1 by our analytical method after being buffered at pH 3.2. These results are consistent with the corresponding community consensus values of 0.090 ± 0.007 nM and 0.67 ± 0.07 nM (Johnson 2007; www.geotraces.org).

3 Results

3.1 Water properties

The two transects (EA1–EA7 and EB1–EB7, Fig. 1) across the shelf–slope interface of the East China Sea were located on a southeast–northwest line from the central Okinawa Trough to the shelf region and on an east–west line from the eastern part of the trough to the shelf, respectively (Table 1). We defined station sites as outer slope, slope, shelf break, and shelf regions (outer slope stations: EA1–EA3; slope stations: EA4 and EA5 and EB1–EB3; shelf break stations: EA6 and EB4 and EB5; shelf stations: EA7 and EB6 and EB7, Table 1). Figures 2a-c and 2d-f show zonal sections of water properties (potential temperature, salinity, and potential density) across the shelf–slope interface along the EA and EB lines, respectively. The corresponding *T/S* diagrams for these transects are shown in Fig. 3a (EA line) and 3b (EB line). The water was categorized into five types: Taiwan Warm Current water (TWCW), shelf mixed water (SMW), Kuroshio surface water (KSW), Kuroshio subsurface water (KSSW), and Kuroshio intermediate water (KIW) (Fig. 3) based on Zhang et al. (2007) and Kodama et al. (2015).

Along the EA line, the sea surface temperature was >25°C. The surface salinity was <34 (TWCW) at EA6 and EA7 and >34 (KSW) at EA1–EA5 (Figs. 2a-c, 3a). The layer immediately beneath KSW was KSSW with a relatively high temperature and the highest salinity of all waters. Salinity >34.75 in the Kuroshio Current was found at

191 depths of 100–250 m at EA1–EA4 (Fig. 2b). Isotherms, isohalines, and isopycnals
192 tilting toward the shelf and upward extended over the slope (Fig. 2a-c), an indication of
193 topographically induced upwelling at the shelf break–slope. In addition, KIW
194 (temperature <15°C and salinity >34.25) was observed at depths of 220–300 m beneath
195 KSSW only at EA5 (bottom depth, 1093 m) along the EA line (Fig. 3a).
196 In contrast, the temperature, salinity, and density stratifications along the EB line
197 were stronger than those along the EA line (Figs. 2, 3). Along the EB line, the sea
198 surface temperature was >25°C, and the surface salinity was <34 (TWCW) at EB2–EB7
199 and >34 (KSW) only at EB1 (Figs. 2d-f, 3b). The SMW and TWCW (salinity <34)
200 intruded into the upper 40 m of the water column at EB2–EB7 (Figs. 2d-f, 3b). In
201 addition, the temperature and salinity in the subsurface water (depths of 70–90 m) at
202 EB1–EB3 were approximately 20 °C and <34.25 (Figs. 2d-e, 3b), respectively, because
203 of intrusion of SMW into the subsurface water. Therefore, the surface and subsurface
204 waters along the EB line, in contrast to the EA line, were strongly influenced by
205 continental shelf waters. The KIW was located between 150 m and 300 m below the
206 surface, beneath KSSW at EB1–EB4 (bottom depths, 203–971 m) (Figs. 2d-f, 3b).
207
208 3.2 Nutrients, apparent oxygen utilization (AOU), and humic F-intensity
209 At EA stations, the surface mixed layer (depths ≤20–30 m) had extremely low nutrient
210 concentrations and AOU: <determination limit–0.2 μM for NO_3+NO_2 (Fig. 4a); ~0.2
211 μM at EA1, EA3, and EA5 and <determination limit–0.05 μM at EA7 for PO_4 (Fig. 4b);
212 2.3–4.1 μM for $Si(OH)_4$ (not shown); and 13–21 μM for AOU (Fig. 4c). However,
213 humic F-intensity values (0.8–1.2 quinine sulfate units [QSU]) in the surface mixed
214 layer at EA7 were approximately twice those (0.3–0.6 QSU) at EA1, EA3, and EA5
215 (Fig. 4d). At depths ≥20–50 m, nutrient concentrations and AOU increased gradually
216 with depth at EA1 and EA3 but more rapidly at EA5 (Fig. 4a-c), whereas humic
217 F-intensities showed similar increasing patterns with depth at EA1, EA3, and EA5 but

218 they at EA7 were nearly uniform and high (1.1–1.2 QSU) throughout the water column
219 (Fig. 4d).
220 At EB stations, the surface mixed layer (depths ≤20–30 m) had extremely low
221 nutrient concentrations and AOU: <determination limit–0.3 μM for NO_3+NO_2 (Fig. 4e);
222 <determination limit–0.3 μM for PO_4 (Fig. 4f); 1.5–4.0 μM for $Si(OH)_4$ (not shown);
223 and 11–16 μM for AOU (Fig. 4g). Humic F-intensity in the surface mixed layer tended
224 to increase toward the shelf, from 0.5–0.6 QSU at EB1 to 0.9–1.2 QSU at EB7 (Fig. 4h).
225 At depths ≥30–50 m, nutrient concentrations and AOU increased rapidly with depth at
226 EB1 and EB3, similar to the pattern at EA5; they increased more rapidly at EB5 and
227 EB7, similar to the pattern at EA7 (Fig. 4a-c, e-g). Humic F-intensity at depths ≥10–30
228 m at all EB stations increased rapidly with depth to a depth of 75 m and then remained
229 high (1.1–1.6 QSU) and relatively uniform below a depth of 75 m (Fig. 4h). The
230 vertical profiles of nutrients and AOU at EB1 and EB3 were very similar to those at
231 EA5 (Fig. 4a-c, e-g).
232
233 3.3 Iron and water transmittance
234 In the surface mixed layer (depths ≤20–30 m) along the EA line, iron concentrations at
235 EA7 were high, ranging from 0.8 to 1.1 nM for D-Fe and from 1.5 to 2.6 nM for TD-Fe,
236 whereas those at EA1, EA3, and EA5 were relatively low, ranging from 0.1 to 0.3 nM
237 for D-Fe and from 0.3 to 0.8 nM for TD-Fe at EA1 and EA3 and from 0.3 to 0.6 nM for
238 D-Fe and from 1.2 to 1.9 nM for TD-Fe at EA5, respectively (Fig. 5a, b). Iron
239 concentrations increased toward the shelf in the surface mixed layer. At EA7 (bottom
240 depth: 116 m), D-Fe concentrations were high (0.7–1.1 nM) and relatively uniform
241 throughout the water column, but TD-Fe concentrations at depths ≥50 m increased
242 rapidly with depth to 22 nM at a depth of 100 m. At depths ≥50–100 m, the iron
243 concentrations at EA1 and EA3 tended to increase slightly with depth [except for the
244 high D-Fe concentration at a depth of 300 m at EA3 (Fig. 5a)], whereas those at EA5

were remarkably high and variable, 1.2–3.3 nM for D-Fe and 3.7-26 nM for TD-Fe (Fig. 5a, b). At each depth below 100 m, the iron concentrations at EA5 were much higher than those at EA1 and EA3; D-Fe was approximately 5–10 times higher and TD-Fe was 10–40 times higher.

In the surface mixed layer (depths ≤20–30 m) along the EB line, iron concentrations at EB5 and EB7 were relatively high, ranging from 0.5 to 1.2 nM for D-Fe and from 0.9 to 2.6 nM for TD-Fe, whereas those at EB1 and EB3 were relatively low, ranging from 0.2 to 0.9 nM for D-Fe and from 1.0 to 1.4 nM for TD-Fe (Fig. 5c, d). The tendency of iron concentrations to increase toward the shelf in the surface mixed layer along the EB line was similar to the pattern along the EA line. In addition, D-Fe concentrations at EB 5 and EB7 (bottom depths: 123 m and 102 m) were high (0.4–1.0 nM and 0.6–1.2 nM, respectively) and relatively uniform throughout the water column (Fig. 5c), similar to those at EA7 (Fig. 5a). However, D-Fe concentrations at EB1 and EB3 decreased gradually with depth in the upper 50 m, reaching minima at a depth of 50 m; they then increased gradually with depth between 50 and 100–125 m and reached relatively uniform concentrations of 0.4–0.7 nM throughout the water column at depths ≥100 m (Fig. 5c). TD-Fe concentrations at depths ≥75 m at EB1 and EB3 increased gradually with depth in the upper 150 m, reaching maxima at a depth of 150 m, and then were relatively uniform, 13–14 nM and 11–19 nM, respectively, below a depth of 150 m. In contrast, TD-Fe concentrations at EB5 and EB7 tended to increase rapidly with depth to values of 60–66 nM and 21–30 nM in bottom waters, respectively (Fig. 5d). The D-Fe and TD-Fe concentrations at depths ≥100 m increased in the order EA5 > EB3 = EB1 > EA3 = EA1 [except for the high D-Fe concentration at a depth of 300 m at EA3 (Fig. 5)].

Vertical profiles of water transmittance (Fig. 6) were mirror images of those of water turbidity, which is contributed by the concentration of suspended particle in the water, as published in previous studies (Takata et al. 2008; Fujita et al. 2010; Kuma et

al. 2014). The fact that water transmittance throughout the water columns along the EA (Fig. 6a) and EB (Fig. 6b) lines was relatively low and variable (89.5–94.2%) at depths ≤100 m was due to the high and variable concentrations of phytoplankton, bacteria, and dissolved organic matter in addition to suspended particles. That the transmittance was high (94.0–94.8%) below a depth of 150 m was due mainly to the relatively low concentration of suspended particles. The water transmittance at depths ≥150 m decreased roughly in the order EA5 > EB3 = EB1 > EA3 = EA1 (Fig. 6).

4. Discussion

4.1 Chemical substances in the surface water

The Changjiang River supplies a large amount of dissolved inorganic nutrients to the East China Sea shelf, resulting in high primary production compared with the outer shelf regions. Nutrient concentrations in East China Sea shelf surface waters gradually decrease from eutrophic coastal to oligotrophic open shelf waters and the gradient depends on the hydrographic stage of the Changjiang River (Zhang et al. 2007). In previous studies (Wang et al. 2016; Zhao et al. 2017), the high concentrations of redox sensitive elements such as Fe^{2+} and Mn^{2+} were found in bottom water and sediment pore-water in the Changjiang Estuary and adjacent inner shelf of the East China Sea but very low concentrations in the central shelf and outer shelf bottom waters. The reductive dissolution of insoluble particulate Fe(III) and Mn(III, IV) oxides were an important early diagenetic pathway, which is largely due to the higher inputs of terrigenous materials from the Changjiang River and abundant reactive organic matter in the Changjiang Estuary and adjacent inner shelf. However, it has been suggested that the dominant source of nutrients to the East China Sea comes from the upwelling of subsurface waters from the Kuroshio Current (Chen 1996; Yang et al. 2013; Lui et al. 2014).

In the present study, phytoplankton growth in the surface mixed layer of the shelf, shelf break, and slope in the East China Sea off the Okinawa Trough may be limited by macronutrient concentrations, which are extremely low, whereas iron concentrations are relatively high (Figs. 4a, b, e, f, 5). The surface water (depths ≤30–40 m) at EA6–EA7 and EB2–EB7 was impacted by the intrusion of TWCW (salinity < 34) from the continental shelf side into the KSW (Figs. 2, 3). The TWCW and KSW are devoid of nutrients although regeneration of nutrients takes place in the near-bottom waters of the inner shelf as a result of extensive bacterial catabolism of organic matter. The approximately linear relationships between humic F-intensities and salinity and between iron concentrations (D-Fe and TD-Fe) and salinity in the upper 30 m at all stations resulted from conservative mixing between TWCW (salinity <34) and KSW (salinity >34), with humic F-intensities and iron concentrations that were relatively high and low, respectively (Figs. 3, 4d, h, 5, 7). Surface water mixing between TWCW and KSW resulted in an increase of humic F-intensity and iron concentration from the shelf via lateral transport of humic-like FDOM and suspended sediment particles from the wide continental shelf (depths ≤200 m), which occupies most of the East China Sea, toward the offshore ocean, where humic-like FDOM and suspended sediment particle concentrations in surface waters are relatively low.

In the present study, humic F-intensities (0.8–1.2 QSU) in surface waters (depths ≤30 m) composed mainly of TWCW were remarkably consistent at shelf stations (EA7 and EB7) (Fig. 4d, h) with those (0.8–1.3 QSU) in Japan Sea surface water, which originates from TWCW and Kuroshio Water, reported in previous studies (Saitoh et al. 2008; Fujita et al. 2010; Kuma et al. 2014). In addition, humic F-intensities (0.3–0.6 QSU) in surface waters composed of KSW at the outer slope and slope stations (EA1, EA3, EA5, EB1, and EB3) were a little higher than those (0.1–0.4 QSU) in the equatorial and central North Pacific surface waters (origin of KSW) (Hayase et al. 1988; Hayase and Shinozuka 1995; Kitayama et al. 2009). In general, the humic F-intensities

326 are low in marine surface waters because of photochemical degradation in the euphotic
327 zone of fluorescent organic matter by sunlight (Mopper et al. 1991; Chen and Bada
328 1992; Nieto-Cid et al. 2006). Humic F-intensities gradually increase with depth because
329 of the formation of fluorescent organic matter during the microbial decomposition of
330 settling particles in the water column (Yamashita and Tanoue 2004; Nieto-Cid et al.
331 2006). In contrast, high humic F-intensities in coastal environments such as TWCW are
332 due to inputs of humic-like FDOM, such as humic and fulvic acids, from rivers and
333 continental shelf sediments as a result of the decomposition of particulate organic
334 matter (Coble 2007; Nishimura et al. 2012; Hioki et al. 2014). In this study, an
335 approximately linear inverse relationship of humic F-intensity to salinity in the surface
336 waters (Fig. 7a) is probably indicating that the humic substances were dominantly
337 derived from riverine input. Numerous studies have shown near linearity of
338 chromophoric dissolved organic matter (CDOM) absorption and humic F-intensity with
339 salinity in estuaries and coastal regions strongly affected by river input, indicating a
340 terrestrial origin for this material and the absence of strong in situ sources and sinks
341 (e.g., de Souza Sierra et al. 1997; Blough and Del Vechio 2002; Del Vecchio and
342 Blough 2004; Coble 2007).
343 In the surface waters, the iron concentrations at outer slope stations (EA1 and
344 EA3) were much lower than those in coastal regions and a little higher than those in the
345 central North Pacific reported in previous studies (Bruland et al. 1994; Saitoh et al.
346 2008; Kitayama et al. 2009; Kuma et al. 2014; Hioki et al. 2014, 2015), because of the
347 relatively low iron inputs from atmosphere and continental shelf to the oligotrophic
348 oceanic surface mixed layer (Figs. 5, 7b, c). The high iron concentrations in the surface
349 waters at shelf and shelf break stations (EA7, EB5, and EB7) are attributable to high
350 iron inputs from atmosphere and upwelled suspended sediment particles into the
351 nutrient-depleted surface water (Fig. 5). Therefore, inverse linear relationships between
352 iron concentrations and salinity and the increase of iron concentrations toward the shelf

353 (Fig. 7b, c) suggest that relatively conservative mixing between shelf and outer shelf
354 surface waters is the major factor controlling the distribution of iron concentration as
355 well as humic F-intensities in the surface water (Fig. 7a).
356
357 4.2 Chemical substances in deep waters
358 Along the EA line, isohalines, isotherms, and isopycnals that shoaled toward the shelf
359 were apparent along the slope (Fig. 2a-c). This pattern is similar to patterns reported in
360 previous studies (Chen et al. 1995; Han et al. 2001) and suggests that there was
361 upwelling of KSSW and KIW along the continental shelf break–slope (Figs. 2a-c, 3a).
362 The upwelling along the EA line contributed to the more abrupt increase of nutrient
363 concentrations, AOUs, and humic F-intensities with increasing depth at slope station
364 EA5 than at the outer slope stations (EA1 and EA3) (Fig. 4a-d). Deep waters below
365 depths of approximately 100 m at the slope stations (EA5, EB1, and EB3) consisted
366 primarily of KIW with relatively high nutrient concentrations, AOUs, and humic
367 F-intensities and relatively low salinity, whereas the analogous waters at the outer slope
368 stations (EA1 and EA3) were composed of KSSW with relatively low nutrient
369 concentrations, AOUs, and humic F-intensities, and relatively high salinity (Figs. 2, 3,
370 4). Similarly, topographically induced upwelling of KIW at the shelf break–slope was
371 indicated by the nutrient concentrations, AOUs, and alkalinity that tilted upward and
372 toward the shelf, as well as by the isotherms, isohalines, and isopycnals which extend
373 over the East China Sea shelf break off northern Taiwan (Chen et al. 1995). It has been
374 reported that NO_3, PO_4, and AOU concentrations in the bottom water on the outer shelf
375 of the East China Sea along a transect across the shelf-slope interface, near the EA line,
376 appear to have increased as KIW contributes substantially to the upwelling (Zhang et al.
377 2007; Lui et al. 2014). The nutrients and AOU concentrations in the upwelled KIW
378 (depths ranging from 150–200 m to 300–400 m) at a slope station (bottom depth:
379 approximately1000 m) ranged from 10 to 20 μM for NO_3, from 0.5 to 1.5 μM for PO_4,

and from 60 to 120 μM for AOU, which were almost the same as those in deep waters (depths ranging from 150 m to 300 m) at the slope stations (EA5, EB1, and EB3) (Fig. 4a-c, e-g). In addition, Minakawa and Watanabe (1998) reported upwelling of Al-poor water originated from the KIW. The intrusion of this water into mid-depths of the Okinawa Trough was apparent from the slopeward decrease of Al concentrations at depths ≤500 m on the continental slope, close to the EA and EB lines in the present study (Fig. 1). In the present study, the abrupt increases in nutrients and AOU concentrations with depth in deep and bottom waters (depths ranging from 30–50 m to 85–115 m) at the shelf and shelf break stations (EA7, EB5, and EB7) (Figs. 4a–c, e–g) may be largely due to the upwelling of KIW along the continental slope and onto the bottom of the shelf–shelf break (Fig. 2) rather than the oxidative decomposition of settling particulate organic matter in the shelf–shelf break bottom water and sediment pore-water. The high TD-Fe concentrations in deep and bottom waters at the shelf and shelf break could result from the resuspension of shelf sediments since the dissolvable particulate Fe (P-Fe) concentrations ([P-Fe]: [TD-Fe] minus [D-Fe]) at the shelf and shelf break stations rapidly increased with depth but D-Fe did not increase (Fig. 5). The abrupt elevated TD-Fe concentration in the shelf–shelf break bottom waters (Fig. 5b, d) may reflect the contribution of the transport across the sediment–water interface of iron species released through the oxidative decomposition of settling particulate organic matter on the shelf–shelf break bottom (Nishimura et al. 2012; Hioki et al. 2014, 2015), besides the upwelling of KIW onto the bottom.

Figure 8 shows the profiles of NO_3+NO_2, AOU, humic F-intensity, and iron concentrations versus potential density and a relationship between NO_3+NO_2 and AOU concentrations at all EA and EB stations. The approximately linear and similar increases in NO_3+NO_2 and AOU concentrations with increasing density at $\sigma\theta \geq 23$ (depths ≥40–50 m) at all stations (Fig. 8a, b) mainly attributed to the upwelling of KIW onto the deep and bottom waters of the shelf–slope (Zhang et al. 2007; Lui et al. 2014). A strong

linear relationship between NO_3+NO_2 and AOU concentrations (Fig. 8c) is substantially due to the nutrient remineralization through the microbial oxidative decomposition of sinking biogenic organic matter in deep water. However, the relationship between humic F-intensity and density ($\sigma\theta$ ranging from ~22 to 24.5: depths ranging from surface to 50–100 m) in deep waters at all EB stations and shelf station EA7 was remarkably different from the approximately linear increases in NO_3+NO_2 and AOU concentrations with increasing density at all stations (Fig. 8a, b) and in humic F-intensity with increasing density at the outer slope and slope stations (EA1, EA3, and EA5) along the EA line (Fig. 8d). The abrupt increases in humic F-intensities with increasing density at $\sigma\theta \leq 24.5$ (Fig. 8d) and the high humic F-intensities at depths ranging from 50 m to 100 m (Fig. 4h) at all EB stations strongly suggest a lateral supply of humic-like FDOM from the shelf to the outer shelf region via intrusion of SMW into KSSW within a narrow depth range (50–100 m) below the surface mixed-layer (Fig. 2d–f) along the EB line (Figs. 2e, 3b). Isobe et al. (2004) reported the intrusion of less saline shelf water into KSSW around the shelf edge of the East China Sea off the Okinawa Trough. The high humic F-intensities in SMW in coastal and shelf environments are possibly due to the large inputs of biologically less active humic-like FDOM from rivers and continental shelf sediments (Coble 2007; Nishimura et al. 2012; Hioki et al. 2014). Humic-like FDOM is largely resistant to direct microbial remineralization although photodegradation is the dominant process for humic-like FDOM removal from natural waters (Blough and Del Vecchio 2002; Coble 2007). Photodegradation of humic-like FDOM by solar radiation is restricted to a very thin surface layer and the effects averaged over a much larger mixing depth. The average penetration depth of the photochemically active UV wavelengths of sunlight becomes comparable to the mixed-layer depth (Blough and Del Vecchio 2002).

The iron concentrations against density at the shelf, shelf break, and slope stations (EA5, EA7, and all EB stations) were much higher and/or variable than those at the

outer slope stations (EA1 and EA3); the concentrations remarkably differed, depending on the station and on the density (Fig. 8e, f). The higher and variable iron concentrations may be largely due to the upwelling of KIW along the continental slope. Previous studies have reported the persistent upwelling of subsurface Kuroshio waters at the shelf break (Chen et al. 1995; Isobe and Beardsley 2006; Zhu et al. 2008). Zhu et al. (2008) and Chen et al. (2017) concluded that some of the terrestrial materials that is transported southward along the Chinese coast turns eastward off the northern Taiwan and subsequently turns around to join the northwardly flowing Kuroshio Current. Finally, the terrestrial material is deposited on the shelf break and slope. In addition, the coastal sediments from China are also transported toward the Kuroshio and the Okinawa Trough in summer by typhoons (Chen et al. 2017). The fine sediments that are deposited on the shelf break and upper slope are then resuspended and brought back to the middle shelf by the strong invasion of subsurface Kuroshio waters close to the bottom. Therefore, high TD-Fe concentrations in deep-bottom waters at the shelf, shelf break, and slope stations (EA5, EA7, and all EB stations) may strongly attribute to the transport of resuspended fine sediments by the upwelling of KIW along the slope and onto the bottom of the shelf–shelf break (Figs. 5b, d, 8f). In the present study, we found strong inverse linear relationships between NO_3+NO_2 concentrations and salinity and between humic F-intensities and salinity in deep waters (depths ≥125 m) at all slope and outer slope stations (Fig. 9a, b). In open ocean, the humic-type FDOM is produced in deep water column by the oxidation and remineralization of settling organic matter, resulting in gradual increase in humic F-intensities with depth, and is destructed by photochemical degradation in the surface waters (Hayase et al. 1988; Chen and Bada 1992). Therefore, the strong linear inverse relationships of humic F-intensity and nutrients to salinity in deep waters at the slope and outer slope stations (Fig. 9b), away from river-dominated margins, simply arise from the conservative mixing of two water masses (KSSW and KIW). However, the relationship between iron concentrations and

461 salinity in deep waters (Fig. 9c, d) was remarkably different from the inverse linearity
462 between nutrient concentrations and humic F-intensities versus salinity. The iron
463 concentrations in deep waters at the slope stations (EA5, EB1, and EB3) were much
464 higher and/or variable, approximately 2–10 times higher for D-Fe concentrations and
465 10–30 times higher for TD-Fe concentrations (Fig. 5), than those at the outer slope
466 stations (EA1 and EA3). Additionally, TD-Fe concentrations in deep waters at the slope
467 stations (Figs. 5b, d, 8f, 9d) were approximately 5–30 times higher than those in the
468 North Pacific Intermediate Water (origin of KIW) in the subtropical North Pacific
469 region (Bruland et al. 1994; Kitayama et al. 2009). Therefore, it is suggested that the
470 remarkably high and variable iron concentrations in deep waters at the slope region are
471 largely due to the transport of iron-rich resuspended fine sediments by the upwelling of
472 KIW along the continental slope.
473
474 4.3 Iron sources
475 The D-Fe concentrations in remote oceanic regions are characteristically low relative to
476 those in coastal environments and may be maintained primarily by complexation of
477 D-Fe with organic Fe-binding ligands such as humic dissolved organic matter, which
478 controls the Fe(III) hydroxide solubility in seawater (Kuma et al. 1996; Tani et al. 2003;
479 Chen et al. 2004; Gerringa et al. 2007; Kitayama et al. 2009; Laglera and van den Berg
480 2009; Hioki et al. 2014). The D-Fe concentrations in the water columns of the shelf,
481 shelf break, slope, and outer stations were variable; the concentrations differed,
482 depending on the station and on the depth or density (Figs 5a, c, 8e). In particular, the
483 D-Fe concentrations at the shelf and shelf break stations (EA7, EB5, and EB7) and in
484 deep water at the slope station (EA5) were remarkably high relative to the solubility of
485 Fe(III); they plotted above the Fe(III) hydroxide solubility–humic F-intensity
486 relationship line (Fig. 10a), which was estimated by fitting a linear equation to the
487 relationship between Fe(III) hydroxide solubility and humic F-intensity in the central

488 North Pacific Ocean (Kitayama et al. 2009). The excess D-Fe concentrations at the shelf
489 and shelf break stations and in deep water at the slope station were probably due to the
490 presence of colloidal Fe in the D-Fe fraction (<0.22 μm pore size) supplied from the
491 resuspended fine sediments which were brought by the upwelling of KIW along the
492 slope and onto the bottom of the shelf–shelf break.
493 The TD-Fe concentrations in the deep waters of the shelf, shelf break, slope, and
494 outer stations were also variable; the concentrations differed, depending on the station
495 and on the depth or density (Fig. 5b, d, 8f). The relative order of the TD-Fe
496 concentrations in deep water (depths ≥150 m) was EA5 > EB3 = EB1 > EA3 = EA1
497 (Fig. 5b, d). This pattern was relatively consistent with the opposite order of water
498 transmittance (Fig. 6). Water absorbance (A) can be expressed as $A = \log_{10} (100/Tr)$.
499 Figure 10b shows the linear relationship between TD-Fe concentrations and A below a
500 depth of 150 m at the slope stations (EA5, EB1, and EB3) and the corresponding
501 relationship at the outer slope stations (EA1 and EA3). The P-Fe concentration in deep
502 water at the slope stations (EA5, EB1, and EB3) was proportional to the concentration
503 of suspended particles, a metric of which would be A. Suspended particles primarily
504 affected light transmission in deep water, although phytoplankton, bacteria, and
505 dissolved organic matter may also have contributed to the reduction of transmittance
506 upper 150 m of the water column (Fig. 6). However, TD-Fe concentrations in deep
507 water at the outer slope stations (EA1 and EA3) were much lower than those at the
508 slope stations and were not likely related to A (Fig. 10b). The implication is that the
509 source of the suspended particles in the region of the outer slope was sinking particulate
510 matter, the source of which is primarily the decomposition of biogenic particulate
511 organic matter in deep water and/or atmospheric inputs. These suspended particles
512 differ from those with high contents of iron found in the slope regions. Therefore, the
513 significant linear relationship of TD-Fe concentration to water transmittance in deep
514 water at the continental slope resulted from the iron supplied to deep water via transport

of iron-rich resuspended sediment by the upwelling of KIW along the slope. Particulate Fe generally having a short residence time may be sensitive to changes in water masses and resuspension of sediments from the continental shelf–slope at various sites in the ocean (Hung et al. 1999; Lam et al. 2006; Lam and Bishop 2008; Zhu et al. 2008; Fujita et al. 2010; Chen et al. 2017).

Acknowledgments We wish to thank the scientists, technicians, captain, and crew of the *T/S Oshoro-Maru* of the Faculty of Fisheries, Hokkaido University for their support in the field observations. Thanks are also extended to two anonymous reviewers for their constructive and helpful comments on this work. A part of this study was supported by Grant-in-Aid for Scientific Research from the Ministry of Education, Culture, Sports, Science and Technology, Japan (no. 22510001).

References

Biller DV, Coale TH, Till RC, Smith GJ, Bruland KW (2013): Coastal iron and nitrate distributions during the spring and summer upwelling season in the central California current upwelling regime. Cont Shelf Res 66:58–72

Blough NV, Del Vecchio R (2002) Chromophoric DOM in the coastal environment. In: Hansell DA, Carlson CA (eds) Biogeochemistry of marine dissolved organic matter. Academic Press, San Diego, pp 509–546

Bruland KW, Orians KJ, Cowen JP (1994) Reactive trace metals in the stratified central North Pacific. Geochim Cosmochim Acta 58:2171–3182

Bruland KW, Rue EL (2001) Analytical methods for the determination of concentrations and speciation of iron. In: Turner DR, Hunter KA (eds) The biogeochemistry of iron in seawater. Wiley, Chichester, pp 255–289

542 Bruland KW, Rue EL, Smith GL (2001) Iron and macronutrients in Californian coastal
543 upwelling regimes: implications for diatom blooms. Limnol Oceanogr
544 46:1161–1674
545 Chen RF, Bada JL (1992) The fluorescence of dissolved organic matter in seawater.
546 Mar Chem 37:191–221
547 Chen CTA (1996) The Kuroshio intermediate water is the major source of nutrients on
548 the East China Sea continental shelf. Oceanol Acta 19:523–527
549 Chen CTA, Ruo R, Pai SC, Liu CT, Wong GTF (1995) Exchange of water masses
550 between the East China Sea and the Kuroshio off northeastern Taiwan. Cont Shelf
551 Res 15:19–39
552 Chen CTA, Kandasamy S, Chang YP, Bai Y, He K, Lu JT, Gao X (2017) Geochemical
553 evidence of the indirect pathway of terrestrial particulate material transport to the
554 Okinawa Trough. Quaternary International 441:51–61
555 Chen M, Wang W-X, Guo L (2004) Phase partitioning and solubility of iron in natural
556 seawater controlled by dissolved organic matter. Global Biogeochem Cycles
557 18:GB4013. doi:10.1029/2003GB002160
558 Chever F, Rouxel OJ, Croot PL, Ponzevera E, Wutting K, Auro M (2015) Total
559 dissolvable and dissolved iron isotopes in the water column of the Peru upwelling
560 regime. Geochim Cosmochim Acta 162:66–82
561 Coble PG (2007) Marine optical biogeochemistry: The chemistry of ocean color. Chem
562 Rev 107:402–418
563 de Baar HJW, de Jong JTM (2001) Distributions, sources and sinks of iron in seawater.
564 In: Turner DR, Hunter KA (eds) The biogeochemistry of iron in seawater. Wiley,
565 Chichester, pp 123–253
566 de Souza Sierra MM, Donard OFX, Lamotte M (1997) Spectral identification and
567 behaviour of dissolved organic fluorescent material during estuarine mixing
568 processes. Mar Chem 58:51–58

569 Del Vecchio R, Blough NV (2004) Spatial and seasonal distribution of chromophoric
570 dissolved organic matter and dissolved organic carbon in the Middle Atlantic
571 Bight. Mar Chem 89:169–187
572 Elord VA, Berelson WM, Coale KH, Johnson KS (2004) The flux of iron from
573 continental shelf sediments: a missing source for global budgets. Geophys Res
574 Lett 31:L12037
575 Elord VA, Johnson KS, Fitzwater SE, Plant JN (2008) A long-term high-resolution
576 record of surface water iron concentrations in the upwelling-driven central
577 California region. J Geophys Res 113:C11021. doi:10.1029/2007JC004610
578 Fujita S, Kuma K, Ishikawa S, Nishimura S, Nakayama Y, Ushizaka S, Isoda Y,
579 Otosaka S, Aramaki T (2010) Iron distributions in the water column of the Japan
580 Basin and Yamato Basin (Japan Sea). J Geophys Res 115:C12001.
581 doi:10.1029/2010JC006123
582 Gerringa LJA, Rijikenberg MJA, Wolterbeek HT, Verburg TG, Bove M, de Baar HJW
583 (2007) Kinetic study reveals weak Fe binding ligand, which affects the solubility
584 of Fe in the Scheld estuary. Mar Chem 103:30–45
585 Han I–S, Kamino K, Matsuno T, Manda A, Isobe A (2001) High frequency current
586 fluctuations and cross-shelf flows around the pycnocline near the shelf break in
587 the East China Sea. J Oceanogr 57:235–249
588 Hayase K, Shinozuka N (1995) Vertical distribution of fluorescent organic matter along
589 with AOU and nutrients in the equatorial Central Pacific. Mar Chem 48:283–290
590 Hayase K, Tsubota H, Sunada I, Goda S, Yamazaki H (1988) Vertical distribution of
591 fluorescent organic matter in the North Pacific. Mar Chem 25:373–381
592 Hioki N, Kuma K, Morita Y, Sasayama R, Ooki A, Kondo Y, Obata H, Nishioka J,
593 Yamashita Y, Nishino S, Kikuchi T, Aoyama M (2014) Laterally spreading iron,
594 humic-like dissolved organic matter and nutrients in cold, dense subsurface water
595 of the Arctic Ocean. Sci Rep 4:6775. doi:10.1038/srep06775

596 Hioki N, Kuma K, Morita Y, Miura D, Ooki A, Tanaka S, Onishi H, Kobayashi N,
597 Kamei Y (2015) Regeneration dynamics of iron and nutrients from bay sediment
598 into bottom water of Funka Bay, Japan. J Oceanogr 71:703–714
599 Hung JJ, Lin CS, Hung GW, Chung YC (1999) Lateral transport of lithogenic particles
600 from the continental margin of the southern East China Sea. Estu Cost Shelf Sci
601 49:483–499
602 Isobe A, Fujiwara E, Chang P–L, Sugimatsu K, Shimizu M, Matsuno T, Manda A
603 (2004) Intrusion less saline shelf water into the Kuroshio subsurface layer in the
604 East China Sea. J Oceanogr 60:853–863
605 Isobe A, Beardsley RC (2006) An estimate of the cross-frontal transport at the shelf
606 break of the east China Sea with the Finite volume coastal ocean model. J
607 Geophys Res 111:C03012
608 Johnson KS, Chavez FP, Elrod VA, Fitzwater SE, Pennigton JT, Buck KR, Walz PM
609 (2001) The annual cycle of iron and the biological response in central California
610 coastal waters. Geophys Res Lett 28:1247–1251
611 Johnson KS (2007) Developing standards for dissolved iron in seawater. EOS Trans
612 AGU 88(11):131–132
613 Kitayama S, Kuma K, Manabe E, Sugie K, Takata H, Isoda Y, Toya K, Saitoh S,
614 Takagi S, Kamei Y, Sakaoka K (2009) Controls on iron distributions in the deep
615 water column of the North Pacific Ocean: Iron(III) hydroxide solubility and
616 marine humic-type dissolved organic matter. J Geophys Res 114:C08019.
617 doi:10.1029/2008JC004754
618 Kodama T, Setou T, Masujima M, Okazaki M, Ichikawa T (2015) Intrusions of excess
619 nitrate in the Kuroshio subsurface layer. Cont Shelf Res 110:191–200
620 Kuma K, Nishioka J, Matsunaga K (1996) Controls on iron(III) hydroxide solubility in
621 seawater: The influence of pH and natural organic chelators. Limnol Oceanogr
622 41:396–407

623 Kuma K, Sasayama R, Hioki N, Morita Y, Isoda Y, Hirawake T, Imai K, Aramaki T,
624 Nakamura T, Nishioka J, Ebuchi N (2014) Chemical evidence for the origin of the
625 cold water belt along the northeastern coast of Hokkaido. J Oceanogr 70:377–387
626 Laglera LM, van den Berg CMG (2009) Evidence for geochemical control of iron by
627 humic substances in seawater. Limnol Oceanogr 54:610–619
628 Lam PJ, Bishop JKB (2008) The continental margin is a key source of iron to the
629 HNLC North Pacific Ocean. Geophys Res Lett 35:L07608,
630 doi:10.1029/2008GL033294
631 Lam PJ, Bishop JKB, Henning CC, Marcus MA, Waychunas GA, Fung IY (2006)
632 Wintertime phytoplankton bloom in the subarctic Pacific supported by continental
633 margin iron. Global Biogeochem Cycles 20: GB1006,
634 doi:10.1029/2005GB002557
635 Lohan MC, Bruland KW (2008) Elevated Fe(II) and dissolved Fe in hypoxic shelf
636 waters off Oregon and Washington: an enhanced source of iron to coastal
637 upwelling regimes. Environ Sci Technol 42:6462–6468
638 Lui H–K, Chen C–TA, Lee J, Bai Y, He X (2014) Looming hypoxia on outer shelves
639 caused by reduced ventilation in the open oceans: Case study of the East China
640 Sea. Estuar Coast Shelf Sci 151:355–360
641 McPhee-Shaw E (2006) Boundary-interior exchange: Reviewing the idea that
642 internal-wave mixing enhances lateral dispersal near continental margins.
643 Deep-Sea Res II 53:42-59
644 Minakawa M, Watanabe Y (1998) Aluminum in the East China Sea and Okinawa
645 Trough, marginal sea areas of the western North Pacific. J Oceanogr 54:629–640
646 Mopper K, Schultz CA (1993) Fluorescence as a possible tool for studying the nature
647 and water column distribution of DOC components. Mar Chem 41:229–238
648 Mopper K, Zhou X, Kieber RJ, Kieber DJ, Sikorski RJ, Jones RD (1991)
649 Photochemical degradation of dissolved organic carbon and its impact on the

650 oceanic carbon cycle. Nature 353:60–62
651 Nedelec F, Statham PJ, Mowlem M (2006) Processes influencing dissolved iron
652 distributions below the surface at the Atlantic Ocean–Celtic Sea shelf edge. Mar
653 Chem 104:156–170
654 Nieto-Cid MA, Ivarez-Salgado XA, Perez FF (2006) Microbial and photochemical
655 reactivity of fluorescent dissolved organic matter in a coastal upwelling system.
656 Limnol Oceanogr 51:1391–1400
657 Nishimura S, Kuma K, Ishikawa S, Omata A, Saitoh S (2012) Iron, nutrients,
658 humic-type fluorescent dissolved organic matter in the northern Bering Sea shelf,
659 Bering Strait, and Chukchi Sea. J Geophys Res 117:C02025.
660 doi:10.1029/2011JC007355
661 Obata H, Karatani H, Nakayama E (1993) Automated determination of iron in seawater
662 by chelating resin concentration and chemiluminescence detection. Anal Chem
663 65:1524–1528
664 Parsons TR, Maita Y, Lalli CM (1984) A manual of chemical and biological methods
665 for seawater analysis. Pergamon, New York
666 Saitoh Y, Kuma K, Isoda Y, Kuroda H, Matsuura H, Wagawa T, Takata H, Kobayashi
667 N, Nagao S, Nakatsuka T (2008) Processes influencing iron distribution in the
668 coastal waters of the Tsugaru Strait, Japan. J Oceanogr 64:815–830
669 Su JL (1998) Circulation dynamics of the China Sea north of 18°N. In: Robinson AR,
670 Brink KH (eds) The sea, vol 11. Wiley, New York, pp 483–505
671 Takata H, Kuma K, Isoda Y, Otosaka S, Senjyu T, Minagawa M (2008) Iron in the
672 Japan Sea and its implications for the physical processes in deep water. Geophys
673 Res Lett 35:L02606. doi:10.1029/2007GL031794
674 Tanaka T, Yasuda I, Kuma K, Nishioka J (2012) Vertical turbulent iron flux sustains
675 the Green Belt along the shelf break in the southeastern Bering Sea. Geophys Res
676 Lett 39:L08603. doi:10.1029/2012GL051164

677 Tani H, Nishioka J, Kuma K, Takata H, Yamashita Y, Tanoue E, Midorikawa T (2003)
678 Iron (III) hydroxide solubility and humic-type fluorescent organic matter in the
679 deep water column of the Okhotsk Sea and the northwestern North Pacific Ocean.
680 Deep-Sea Res I 50:1063–1078
681 Wang Z–W, Ren J–L, Jiang S, Liu S–M, Xuan J–L, Zhang J (2016) Geochemical
682 behavior of dissolved manganese in the East China Sea: Seasonal variation,
683 estuarine removal, and regeheration under suboxic conditions. Geochem Geophys
684 Geosyst 17:282–299, doi:10.1002/2015GC006128
685 Yamashita Y, Tanoue E (2004) In situ production of chromophoric dissolved organic
686 matter in coastal environments. Geophys Res Lett 31:L14302.
687 Yang D, Yin B, Sun J, Zhang Y (2013) Nurmerical study on the origins and the forcing
688 mechanism of the phosphate in upwelling areas off the coast of Zhejiang province,
689 China in summer. J Mar Syst 123–124:1–18
690 Zhang J, Liu SM, Ren JL, Wu Y, Zhang GL (2007) Nutrient gradients from the
691 eutrophic Changjiang (Yangtze River) Estuary to the oligotrophic Kuroshio waters
692 and re-valuation of budgets for the East China Sea Shelf. Prog Oceanogr
693 74:449–478
694 Zhao B, Yao P, Bianchi TS, Xu Y, Liu H, Mi T, Zhang X–H, Liu J, Yu Z (2017) Early
695 diagenesis and authigenic mineral formation in mobile muds of the Changjiang
696 Estuary and adjacent shelf. J Mar Syst 172:64–74
697 Zhu C, Xue B, Pan J, Zhang H, Wagner T, Pancost RD (2008) The dispersal of
698 sedimentary terrestrial organic matter in the East China Se (ECS) as revealed by
699 biomarkers and hydro-chemical characteristics. Organic Geochem 39:952–957
700
701
702 Figure legends
703 **Fig. 1** Station locations along two transects in the East China Sea off the Okinawa

Trough. The two transects included seven stations (EA1–EA7) along the EA line (27°09′–29°00′N, 126°00′–127°00′E) and seven stations (EB1–EB7) along the EB line (29°43′N, 126°45′–128°15′E) (Table 1). The orange and red arrows show the Taiwan Warm Current and the Kuroshio Current, respectively. Water samples were collected at four stations (EA1, EA3, EA5, and EA7) along the EA line and at four stations (EB1, EB3, EB5, and EB7) along the EB line.

Fig. 2 Vertical distributions of potential temperature (θ), salinity (S), and potential density (σ_θ) across the shelf-slope interface [EA line (a, b, c) and EB line (d, e, f)] in the East China Sea off the Okinawa Trough.

Fig. 3 Relationship between potential temperature and salinity at stations EA1, EA3, EA5, and EA7 along the EA line (a) and at stations EB1, EB3, EB5, and EB7 along the EB line (b). The relationships reveal five water masses that originate from the Taiwan Warm Current and the Kuroshio Current (TWCW: Taiwan Warm Current water; SMW: shelf mixed water; KSW: Kuroshio surface water; KSSW: Kuroshio subsurface water; KIW: Kuroshio intermediate water).

Fig. 4 Vertical distributions of NO_3+NO_2 concentrations (a, e), PO_4 concentrations (b, f), AOU (c, g), and humic F-intensity (d, h) at the EA stations on 3–4 July 2011 (a, b, c, d) and at the EB stations on 1–2 June 2011 (e, f, g, h). Hatched rectangles indicate bottom depths at the shelf stations.

Fig. 5 Vertical distributions of dissolved iron (D-Fe) concentration (a, c) and total dissolvable iron (TD-Fe) concentration (b, d) at the EA stations (a, b) and the EB stations (c, d). Hatched rectangles indicate bottom depths at the shelf stations.

731 **Fig. 6** Vertical profiles of water transmittance at the EA stations (a) and the EB stations
732 (b). Hatched rectangles indicate bottom depths at the shelf stations.
733
734 **Fig. 7** Humic F-intensity (a), D-Fe (b), and TD-Fe (c) versus salinity at depths 30 m at
735 all EA and EB stations. Each solid line is a linear regression of the data in the panel.
736
737 **Fig. 8** NO_3+NO_2 (a), AOU (b), humic F-intensity (d), D-Fe (e), and TD-Fe (f) versus
738 salinity and NO_3+NO_2 versus AOU (c) at all EA and EB stations. Each solid line is a
739 linear regression of the data in the panel.
740
741 **Fig. 9** NO_3+NO_2 (a), humic F-intensity (b), D-Fe (c), and TD-Fe (d) versus salinity at
742 depths ≥125 m at all EA and EB stations. The solid lines are linear regression for
743 relationships between NO_3+NO_2 and salinity and between humic F-intensity and
744 salinity.
745
746 **Fig. 10** Relationships between D-Fe and humic F-intensity in the water column (a) and
747 between TD-Fe and water absorbance at depths ≥150 m (b) at all EA and EB stations.
748 The solid line in (a) indicates the Fe(III) hydroxide solubility as estimated by fitting a
749 linear equation to the relationship between Fe(III) hydroxide solubility (nM) and humic
750 F-intensity (QSU) in the central North Pacific Ocean: Fe(III) hydroxide solubility =
751 0.226 × humic F-intensity – 0.045; R = 0.78, n = 14 (Kitayama et al. 2009). The solid
752 line in (b) is a linear regression of all data from the shelf break stations (EA5, EB1, and
753 EB3), except for the outer shelf break stations (EA1 and EA3).
754
755
756 **Table 1** Latitudes and longitudes, bottom depths, sites, and sampling dates of stations
757 EA1–EA7 and EB1–EB7 in the East China Sea.

Table 1. Latitudes and longitudes, bottom depths, sites, and sampling dates of stations EA1–EB7 and EB1–EB7 in the eastern East China Sea. Star (*) mark shows the water sampling stations.

	Position				
	Latitude	Longitude	Bottom Depth (m)	Station Site	Sampling Date
Station	(N)	(E)			
(EA line)					
*EA1	27°09.13'	127°00.25'	1,537	Outer slope	4.Jul.11
EA2	27°18.40'	126°48.33'	1,615	Outer slope	3.Jul.11
*EA3	27°26.10'	126°37.78'	1,607	Outer slope	3.Jul.11
EA4	27°33.77'	126°28.89'	1,404	Slope	3.Jul.11
*EA5	27°41.80'	126°16.83'	1,093	Slope	3.Jul.11
EA6	27°50.87'	126°07.80'	133	Shelf break	3.Jul.11
*EA7	27°59.86'	125°59.86'	116	Shelf	3.Jul.11
(EB line)					
*EB1	29°42.63'	128°15.16'	971	Slope	1.Jul.11
EB2	29°42.65'	128°00.12'	717	Slope	1.Jul.11
*EB3	29°42.60'	127°44.98'	555	Slope	1.Jul.11
EB4	29°42.05'	127°30.01'	203	Shelf break	1.Jul.11
*EB5	29°42.50'	127°14.97'	123	Shelf break	1.Jul.11
EB6	29°42.68'	126°59.93'	108	Shelf	1.Jul.11
*EB7	29°42.83'	126°44.83'	102	Shelf	2.Jul.11

Fig. 1 Sasayama et al.

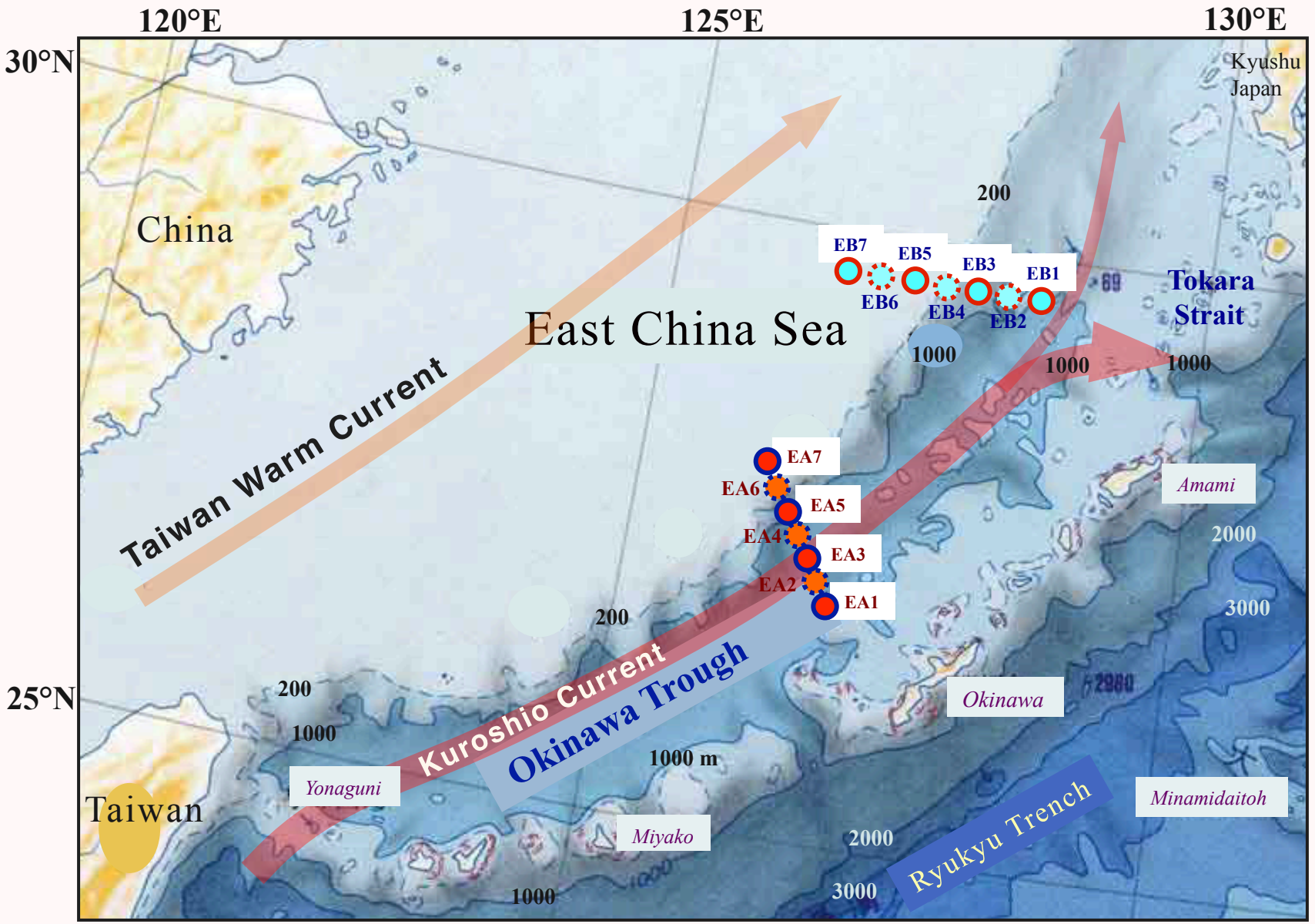

Fig. 2 Sasayama et al.

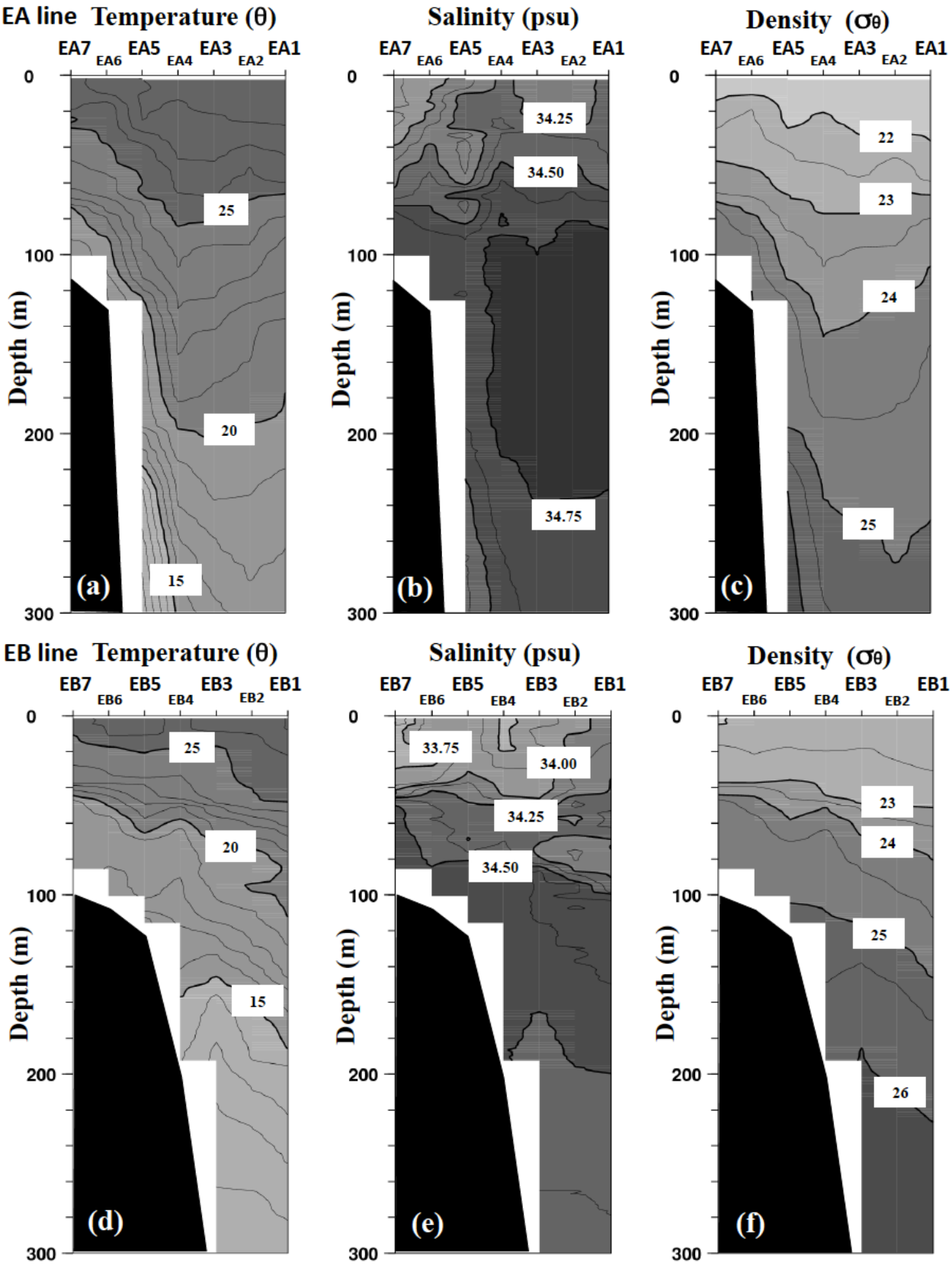

Fig. 3 Sasayama et al.

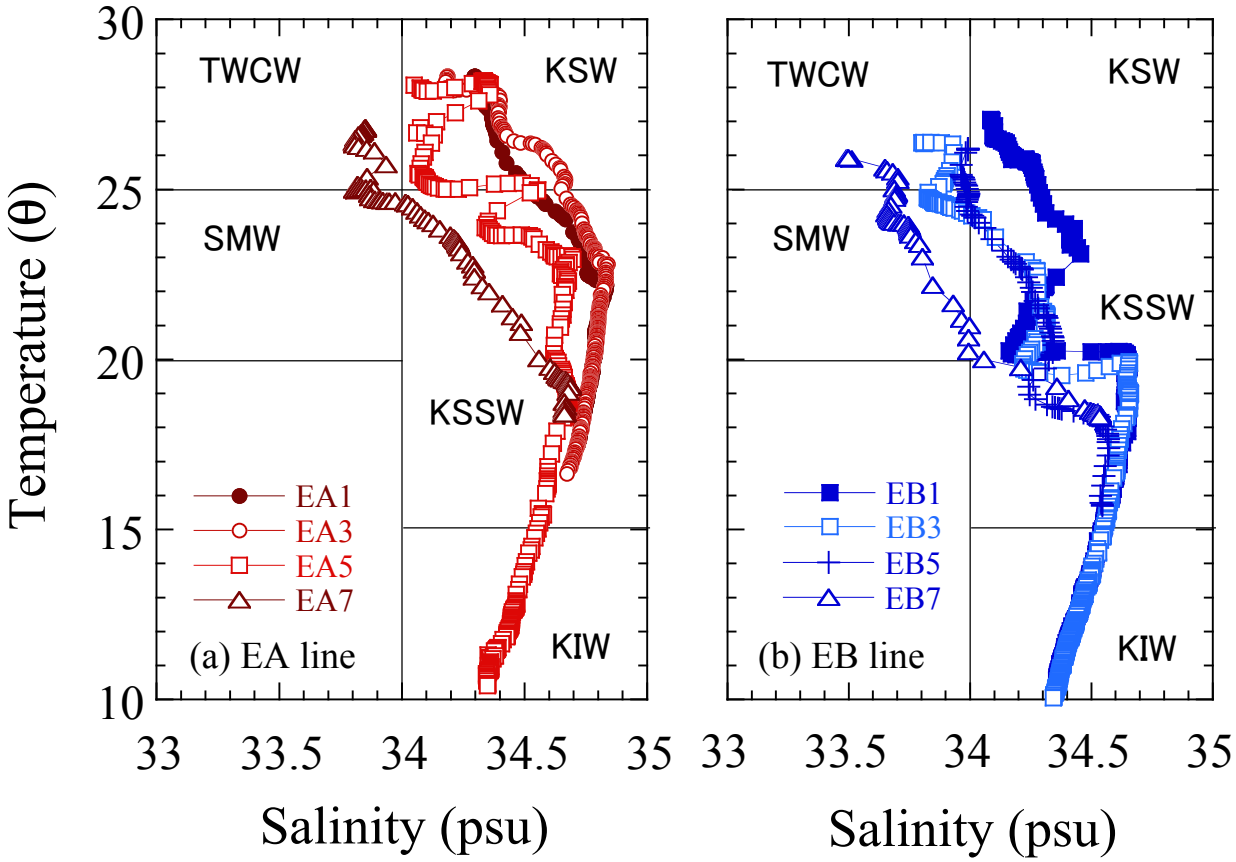

Fig. 4 Sasayama et al.

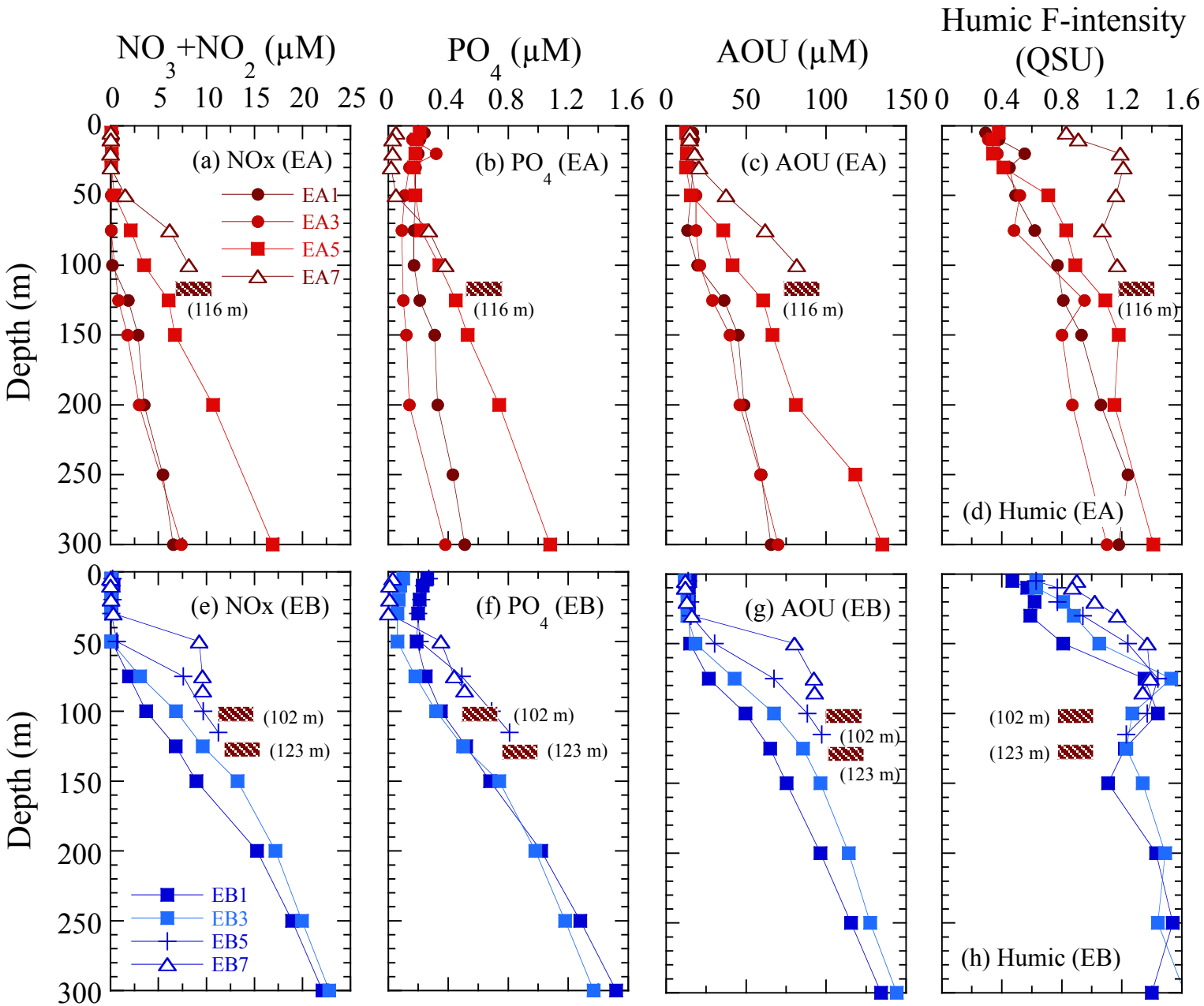

Fig. 5 Sasayama et al.

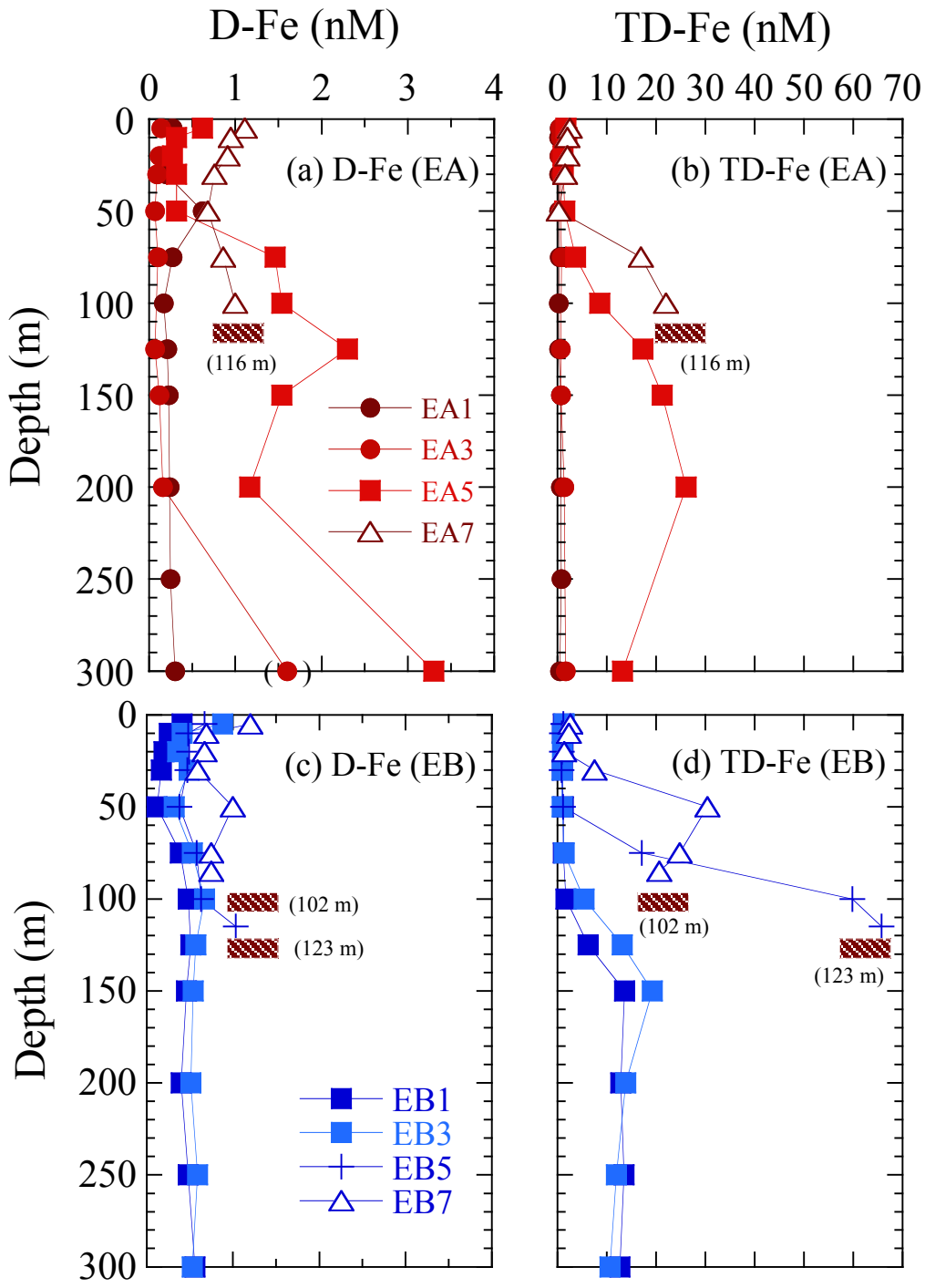

Fig. 6 Sasayama et al.

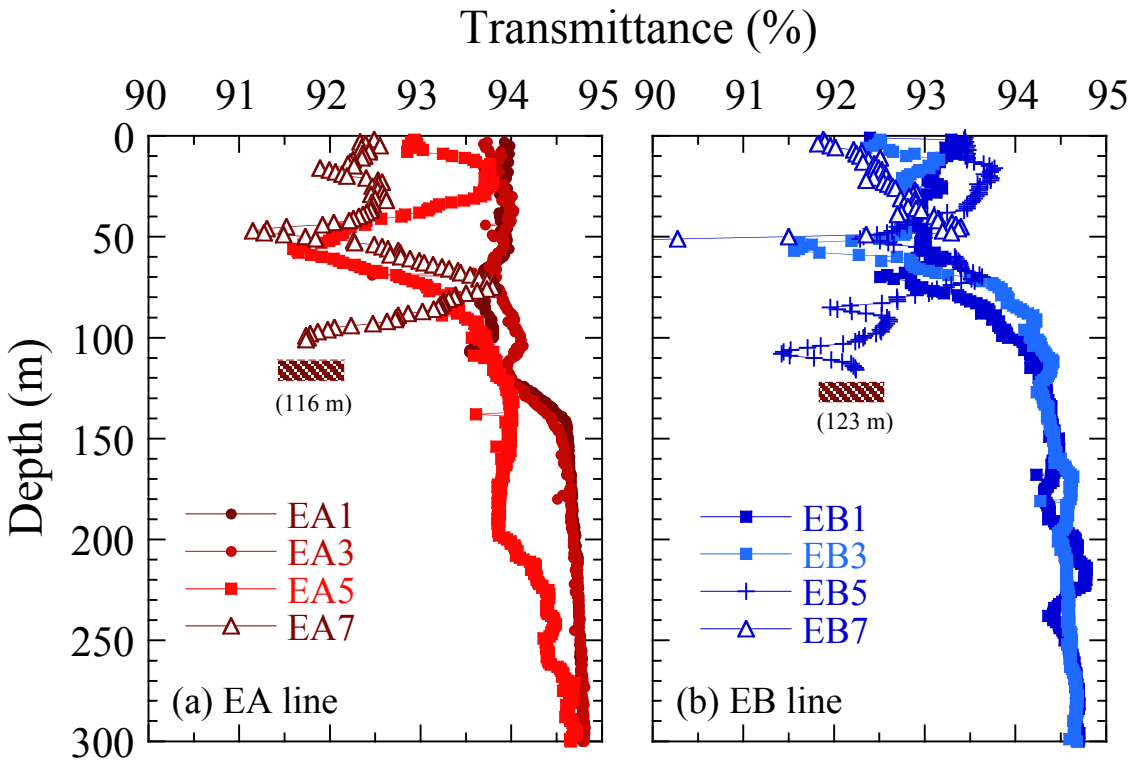

Fig. 7 Sasayama et al.

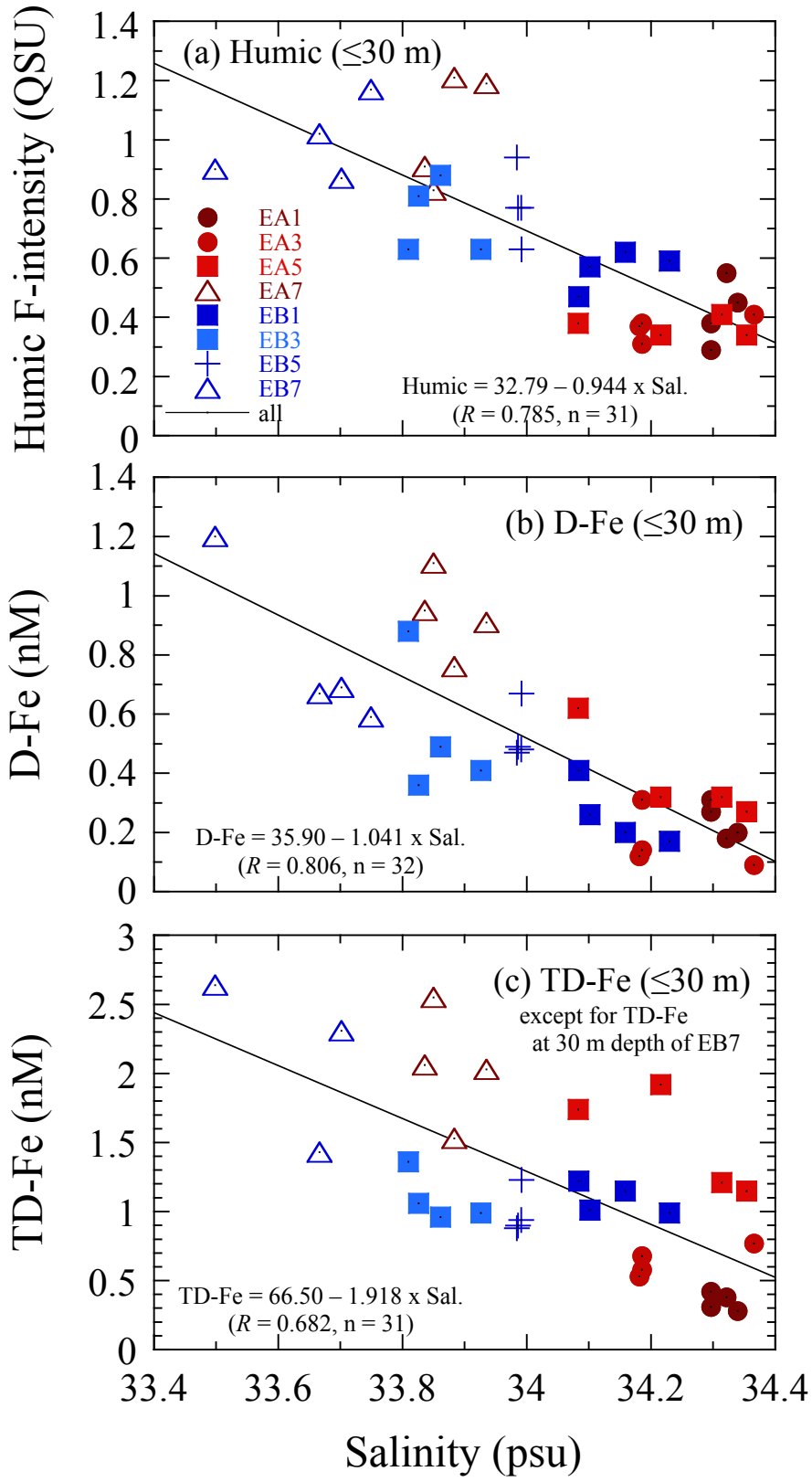

Fig. 8 Sasayama et al.

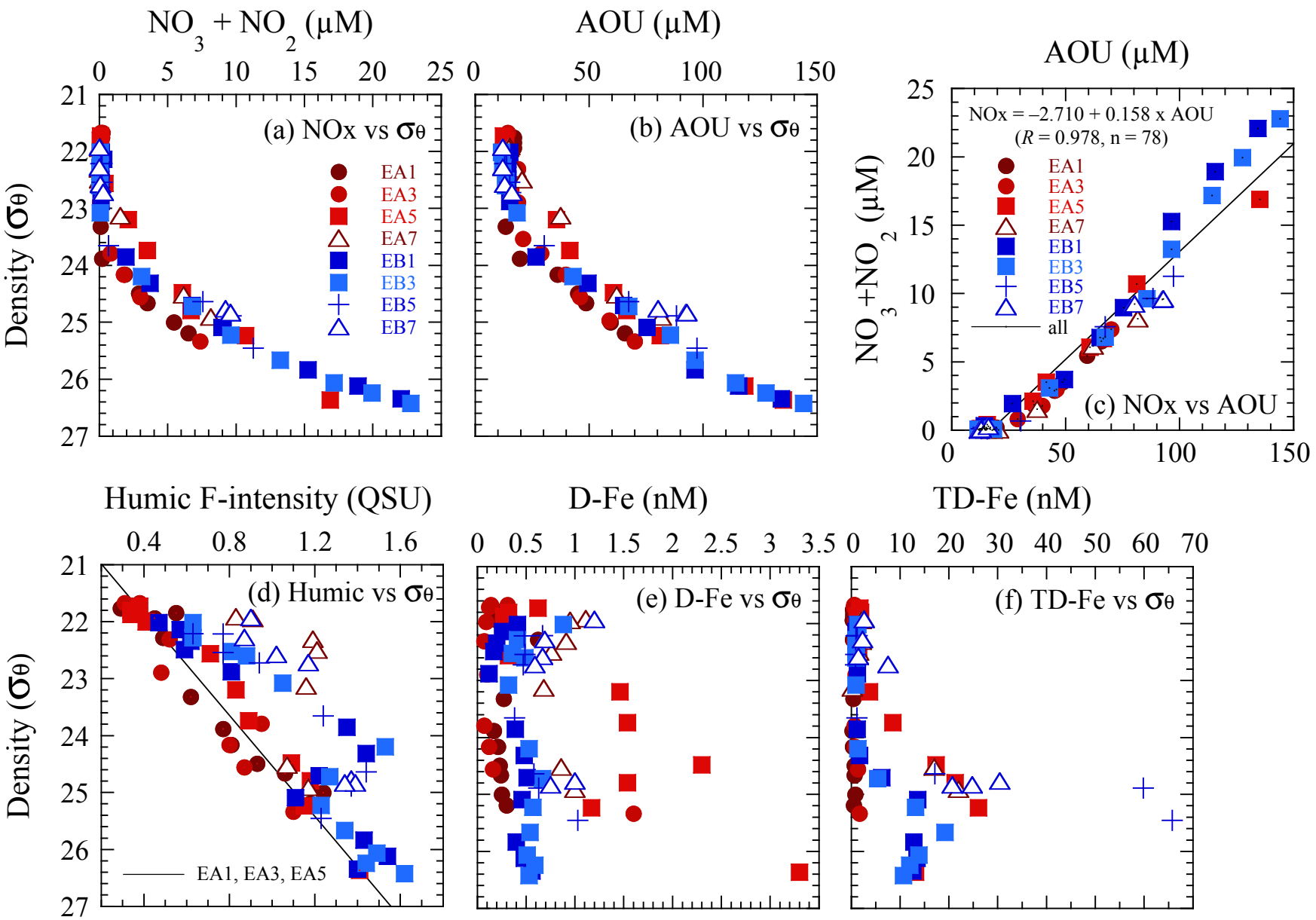

Fig. 9 Sasayama et al.

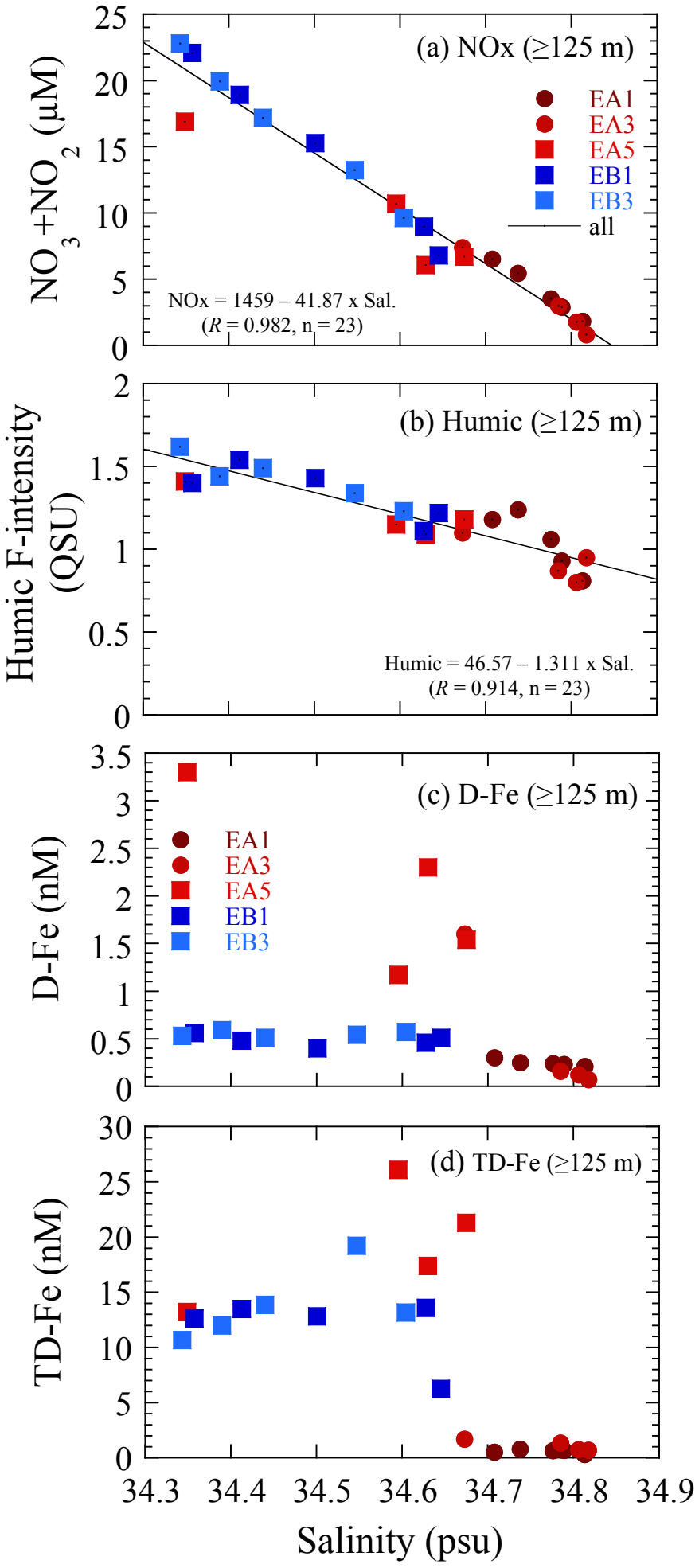

Fig. 10 Sasayama et al.